A Strength of Materials Formulation for Thin Walled Composite Beams with Torsion

JULIO C. MASSA
National University of Cordoba
Argentina

EVER J. BARBERO*
Department of Mechanical and Aeronautic Engineering
315 Engineering Science Building
West Virginia University
Morgantown, WV 26506

(Received March 30, 1997)
(Revised September 25, 1997)

ABSTRACT: A simple methodology for the analysis of thin walled composite beams subjected to bending, torque, shear, and axial forces is developed. Members with open or closed cross section are considered. The cross section is modeled as a collection of flat, arc-circular, and concentrated area segments. Each laminated segment is modeled with the constitutive equations of classical lamination theory accounting for a linear distribution of normal and shear strains through the thickness of the walls, thus allowing for greater accuracy than classical thin walled theory when the walls are moderately thick. The geometric properties used in classical beam theory such as area, first moment of area, center of gravity, etc., are no longer used because of the variability of the materials properties in the cross section. Instead, mechanical properties such as axial stiffness, mechanical first moment of area, mechanical center of gravity, etc., are defined to incorporate both the geometry and the material properties. Warping, restriction to warping, and secondary stresses are considered. Failure predictions are made with customary failure criteria. Comparison with experimental results are presented.

1. INTRODUCTION

COMPOSITE MATERIALS ARE being used in all types of structural applications, from aircraft structures to civil infrastructure [1]. Beams, which constitute the most common structural component, are subjected to combined loading including bending,

*Author to whom correspondence should be addressed.

0021-9983/98/17 1560–36 $10.00/0

shear, torsion, and axial forces. From a design point of view, there is considerable interest in developing a beam theory including torsion that results in simple equations similar to those available for beams made of a single isotropic and homogeneous material. Beam theories attempting to address the case of generally laminated section with arbitrary geometry result in complex formulations for which solutions can be obtained only in a limited number of simple cases. A general formulation is presented in Reference [2], and the equations are solved for a solid rectangular layered section. Analytical solutions exist for the case of two-layer isotropic [3], symmetric sandwich isotropic [4], homogeneous anisotropic [5], and laminated bars [6,7]; with all these solutions limited to rectangular solid sections.

Introducing approximations regarding the kinematics of deformation in the laminate, it is possible to obtain simpler solutions to more general cases, although the accuracy may suffer for cases of strong material coupling. Approximate formulations are developed in Reference [8], separately for the cases of rectangular, tubular, and open sections. An approximate formulation for rectangular beams is presented in Reference [9] and closed form solutions are derived for the specially orthotropic laminated beam. Using first order shear deformation theory (FSDT) to model the kinematics of the laminate, a closed form solution to a general orthotropic laminate is developed in Reference [10] for rectangular solid geometry. FSDT was also used in Reference [11] to develop the differential equations governing the beam behavior of thin-walled laminated sections which are then solved for the case of circular cylindrical shells. A simple formulation was presented in Reference [28] to compute the bending and shear stiffness of Timoshenko's beam theory for thin-walled laminated beams without torsion. Fortunately, many practical engineering applications exist for which the approximations made in these theories are reasonable. These include the cases of pultruded structural shapes widely used in civil infrastructure applications, and most laminated beams where thick laminates, very dissimilar materials, or severely unsymmetrical, unbalanced lay-ups are excluded to avoid the undesirable effects that those configurations produce, including warping due to curing residual stresses, etc.

Of course, special applications do exist, such as helicopter rotor blades [12], and swept forward aircraft wings [13], were strong coupling effects are desirable. No attempt is made in this work to address these complex situations. Solutions are also available for special geometries, specially cylindrical shells [14]. Contour analyses for aeroelastically tailored composite rotor blades are presented in References [15–17]. Direct solution of the governing differential equations was accomplished for the case of single-cell closed section in Reference [18] and [16]. Reduced plate models have been used for composite box beams [19,20].

Experimental results for laminated circular pipe are presented in Reference [21] along with analysis of the results. Experimental results for rectangular tubes made of Graphite-Epoxy are reported in Reference [22]. Analysis and comparison with the experimental results is presented in Reference [23]. Both papers deal with

box-beams exhibiting bending-torsion coupling, extension-shear coupling, extension-torsion coupling, and bending-shear coupling, typical of helicopter rotor blades. While strong coupled behavior is common in helicopter rotor blades, it is not common in most structural applications such as civil construction, automotive, etc., because coupling leads to undesirable residual stresses and warping during manufacturing.

The objective of this investigation is to develop simple equations that can be used for design of open or closed sections of arbitrary shape. In order to arrive at practical equations, the off-ply layers should be arranged in a balanced symmetric configuration. The laminate can be unsymmetrical as a result of orthotropic layers (isotropic, unidirectional, or random reinforced layers) that are not symmetrically arranged with respect to the middle surface.

2. DESCRIPTION OF THE CROSS SECTION

The cross section is described by the contour, which is a line going through the midsurface of all the panels that form the cross section (Figure 1). Each panel is described by one or more segments. One segment is used for each panel in Figure 2a. Two segments or more are necessary for each flange in Figure 2b because a node must be placed at the flange-web connection. From now on we will refer to seg-

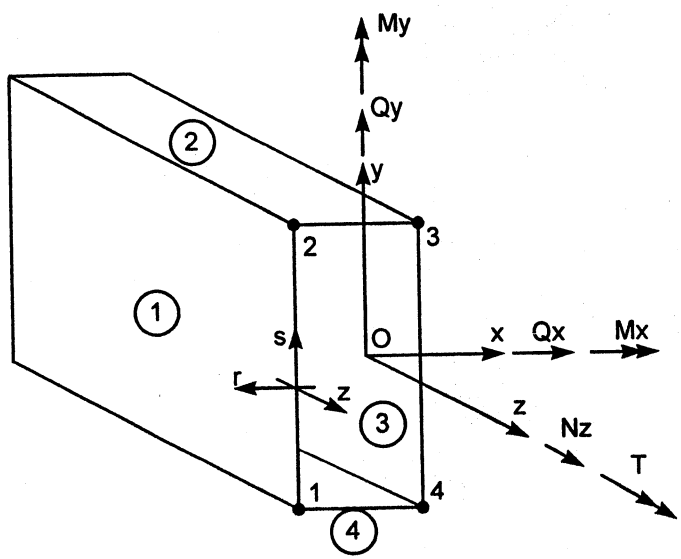

Figure 1. *Definition of the global and local coordinate systems, and node and segment numbering for a symmetric, closed section.*

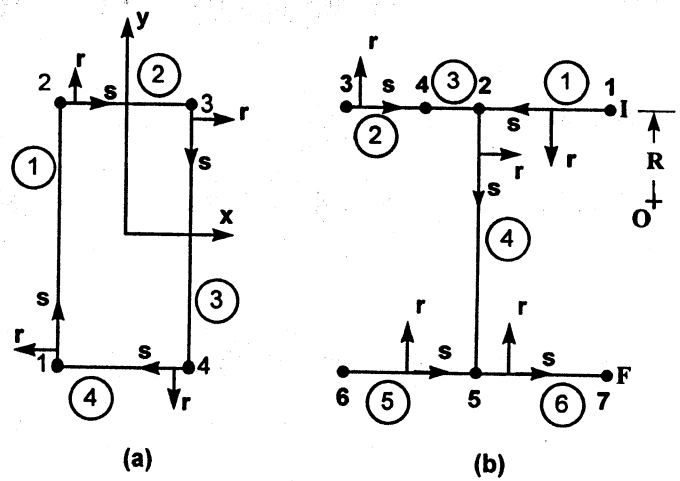

Figure 2. *Definition of the local coordinate system, node and segment numbering for (a) a closed section, (b) and open section.*

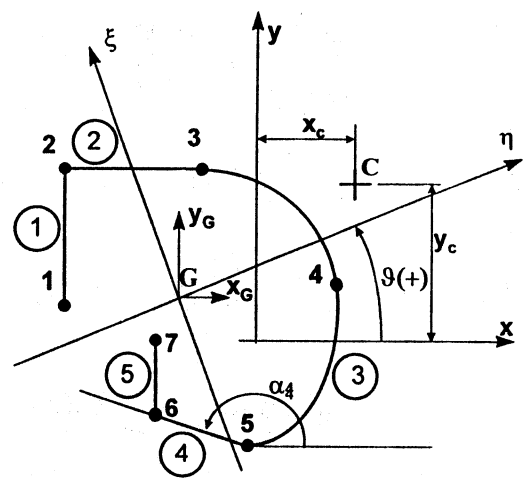

Figure 3. *Definition of principal axes of bending for a general open section.*

Table 1. Contour definition for Figure 2a.

Segment Number	n_i	n_f	Segments Converging to n_i		
1	1	2	0	0	0
2	2	3	1	0	0
3	3	4	2	0	0
4	4	1	3	0	0

ments instead of panels to describe each flat or curve wall composing the thin walled beam because the term panel is used in many engineering disciplines to describe such things as stiffened panels in ship or aircraft construction, bridge panels, etc. The segments can be flat or curved in the shape of an arc of circle (Figure 3). Concentrated areas can be added to represent the contributions of attachments that we do not choose to model explicitly. Arc segments are divided in a large number of flat segments for analysis.

The definition of each segment is done in terms of the nodes, which can be numbered arbitrarily. All segments are defined by an initial node n_i and a final node n_f. Arc-circular segments need a third mid-node to define the geometry. For a closed section, the segments and the nodes are numbered consecutively. Reference must be made to all the segments converging to the initial node of each segment**. Table 1 summarizes the description of the contour shown in Figure 2a. Table 2 summarizes the description of the contour shown in Figure 2b.

The contour integrals are done segment by segment, accumulating the contribution of all the segments. The order in which segments are defined and the orientation of the s-coordinate in each segment must allow for the correct accumulation of contour integrals such as first moment of area, which must start at a free end. Taking Figure 2b and Table 2 as an example, note that the definition of the segments 1 and 2 start at a free edge with the s-coordinate oriented towards the common node.

**The current computer implementation allows for up to three predefined segments to converge to the initial node n_i of any segment (see Table 1 and 2).

Table 2. Contour definition for Figure 2b.

Segment Number	n_i	n_f	Segments Converging to n_i		
1	1	2	0	0	0
2	3	4	0	0	0
3	4	2	2	0	0
4	2	5	1	3	0
5	6	7	0	0	0
6	5	7	4	5	0

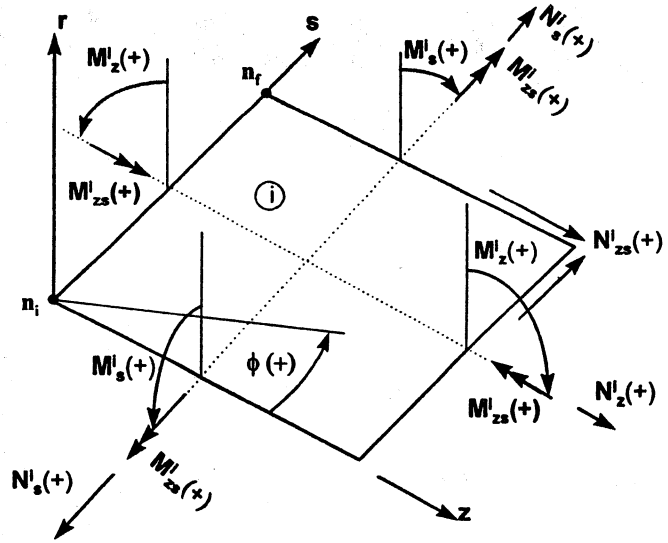

***Figure 4.** Definition of stress resultants in the laminate.*

Segment 4 is defined with the common node (node 2) as the initial node. Segments 1 and 3 must be defined as converging to segment 4, so that the contour integral for the static moment will accumulate the contribution of the previous segments. A segment with a free edge can be defined at any time with the free edge as the first node (n_i) with the exception of segment 6 where the free edge is the final node of the segment to complete the contour integral. Note that the local coordinates are oriented from n_i to n_f, resulting in opposite orientation in segments 1 and 2. This has an important implication in the way the laminate is defined because the first layer is always at the surface with negative r-coordinate.

The coordinates of each node are given in terms of an arbitrarily selected global coordinate system. The global coordinate system is shown in Figure 1 and Figure 3, with axes z, x, y. In Figure 3, the coordinate system η, ξ, rotated and angle ϑ with respect to the global coordinate system, describes the principal axes of bending.

Each segment also has its own local coordinate system (Figure 2). The contour coordinate s is oriented from the initial node to the final node. The other two local coordinates are the global z-axis and the r-axis that is obtained as the cross product of z times s, or $r = z \times s$, in such a way that the r-coordinate spans the thickness of the segment.

The fiber orientation of layer k is given by the angle ϕ^k (Figure 4) which is positive counterclockwise around the r-axis and starting from the z-axis. While the

z-axis always coincides with the axis of the beam, the r-axis orientation depends on the nodes n_i and n_f. The first layer ($k = 1$), of thickness t^k, is located at the bottom of the laminate, on the negative r-axis. It is important to emphasize that if one segment orientation is changed; a) the order of the laminas in that segment must be changed and b) the sign of each lamina orientation angle ϕ^k in that segment must also be changed.

3. SEGMENT STIFFNESS

Each segment of the cross section is modeled initially as a thin plate using the constitutive equations of a laminated plate, neglecting transverse shear deformation

$$\begin{Bmatrix} N_z^i \\ N_s^i \\ N_{zs}^i \\ M_z^i \\ M_s^i \\ M_{zs}^i \end{Bmatrix} = \begin{bmatrix} A_{11} & A_{12} & A_{16} & B_{11} & B_{12} & B_{16} \\ & A_{22} & A_{26} & B_{12} & B_{22} & B_{26} \\ & & A_{66} & B_{16} & B_{26} & B_{66} \\ & & & D_{11} & D_{12} & D_{16} \\ & & & & D_{22} & D_{26} \\ sym. & & & & & D_{66} \end{bmatrix} \begin{Bmatrix} \varepsilon_z^i \\ \varepsilon_s^i \\ \gamma_{zs}^i \\ \kappa_z^i \\ \kappa_s^i \\ \kappa_{zs}^i \end{Bmatrix} \tag{1}$$

where the superscript $(\,)^i$ indicates the segment number, A_{pq} are the inplane stiffness, B_{pq} are the coupling stiffnesses, and D_{pq} are the out-of-plane stiffnesses (see References [24,25]), with $p, q = 1, 2, 6$.

In Equation (1), N_z^i, N_s^i, and N_{zs}^i are the tensile and shear forces per unit length along the boundary of the plate (Figure 4) with units [N/m], M_z^i, M_s^i, M_{zs}^i are the moments per unit length on the sides, with units [N]. The bending moments are positive when they produce a concave deformation looking from the negative r-axis. The mid-plane strains are ε_z^i, ε_s^i, and γ_{zs}^i, and the curvatures are κ_z^i, κ_s^i, and κ_{zs}^i. Note that from equilibrium $\sigma_{sz} = \sigma_{zs}$. Therefore, only M_{zs} will be used in the rest of this paper, with the orientation given in Figure 4.

The superscript $(\,)^i$ is used not only to indicate the segment number but also to differentiate the plate quantities $N_z^i, N_s^i, N_{zs}^i, M_z^i, M_s^i, M_{zs}^i, \varepsilon_z^i, \varepsilon_s^i, \gamma_{zs}^i, \kappa_z^i, \kappa_s^i$, and κ_{zs}^i (which vary along the contour, see Figure 4) from the constant beam quantities *N_z, Q_η, Q_ξ, M_z, M_η, M_ξ, ε_z, κ_η, κ_ξ, and β (see Figure 1) to be defined later. Plate stress resultants (forces and moments per unit length) and strains are function of the contour coordinate s and must be interpreted as $N_z^i(s)$, $N_s^i(s)$, $\varepsilon_z^i(s)$, $\varepsilon_s^i(s)$, etc., in the rest of the paper.

The stiffness equations (i.e., ABD matrix) are inverted to get the compliance equations

$$\begin{Bmatrix} \varepsilon_z^i \\ \varepsilon_s^i \\ \gamma_{zs}^i \\ \kappa_z^i \\ \kappa_s^i \\ \kappa_{zs}^i \end{Bmatrix} = \begin{bmatrix} \alpha_{11} & \alpha_{12} & \alpha_{16} & \beta_{11} & \beta_{12} & \beta_{16} \\ & \alpha_{22} & \alpha_{26} & \beta_{12} & \beta_{22} & \beta_{26} \\ & & \alpha_{66} & \beta_{16} & \beta_{26} & \beta_{66} \\ & & & \delta_{11} & \delta_{12} & \delta_{16} \\ & & & & \delta_{22} & \delta_{26} \\ sym. & & & & & \delta_{66} \end{bmatrix} \begin{Bmatrix} N_z^i \\ N_s^i = 0 \\ N_{zs}^i \\ M_z^i \\ M_s^i = 0 \\ M_{zs}^i \end{Bmatrix} \tag{2}$$

Equations 1 and 2 contain the plane stress assumption $\sigma_r = 0$. Next, the undeformability of the contour is used, as in classical thin walled theory, to further reduce the complexity of the problem. Tsai [26] used the elements of the compliance matrix in Equation (2) to define inplane and flexural engineering constants for a laminate, effectively setting all but one of the stress resultants in the right hand side of Equation (2) to define each coefficient. Wu and Sun [27] showed that using the assumption $N_s^i = M_s^i = 0$ for slender, thin-walled laminated beams yields more accurate results than the alternative plane strain assumption $\varepsilon_s^i = \kappa_s^i = 0$. Therefore, we assume

$$N_s^i = M_s^i = 0 \tag{3}$$

which is an approximation. This assumption was also used in Reference [28] to develop a theory for laminated thin walled beams of symmetric cross-section subject to bending only. The results of such theory compare favorably with experimental data [29] and finite element results [28, 30, 31]. Then, by virtue of Equation (3), the second and fifth column of the compliance matrix [Equation (2)] are not used, and retaining only the terms that are of interest we get

$$\begin{Bmatrix} \varepsilon_z^i \\ \gamma_{zs}^i \\ \kappa_z^i \\ \kappa_{zs}^i \end{Bmatrix} = \begin{bmatrix} \alpha_{11} & \alpha_{16} & \beta_{11} & \beta_{16} \\ \alpha_{16} & \alpha_{66} & \beta_{16} & \beta_{66} \\ \beta_{11} & \beta_{16} & \delta_{11} & \delta_{16} \\ \beta_{16} & \beta_{66} & \delta_{16} & \delta_{66} \end{bmatrix} \begin{Bmatrix} N_z^i \\ N_{zs}^i \\ M_z^i \\ M_{zs}^i \end{Bmatrix} \tag{4}$$

If the laminate has off-axis plies that are balanced symmetric, then $\alpha_{16} = \beta_{16} = 0$. The term δ_{16} is zero for laminates made with specially orthotropic layers. When the off-axis plies are made with intermingled or stitched $\pm\theta$ layers of fabric, each layer of fabric is specially orthotropic and $\delta_{16} = 0$ for the laminate. To reduce manufacturing costs, many composites are now made with stitched fabrics that contain two inter-mingled $\pm\theta$ layers in one layer instead of stacking two layers of prepreg tape. Then, the laminate is usually made symmetric to avoid warping due to residual

stresses created during curing of the material. If the laminate needs to be unsymmetrical, it is usually because of the addition of isotropic or 0/90 pair of layers. Under these conditions $\delta_{16} = 0$. Otherwise, δ_{16} decreases rapidly in magnitude when the number of off-axis, balanced symmetric layers increases [24]. Then, assuming uncoupling between normal and shearing effects, the compliance equation [Equation (4)] can be written as

$$\begin{Bmatrix} \varepsilon_z^i \\ \kappa_z^i \\ \gamma_{zs}^i \\ \kappa_{zs}^i \end{Bmatrix} = \begin{bmatrix} \alpha_{11} & \beta_{11} & 0 & 0 \\ \beta_{11} & \delta_{11} & 0 & 0 \\ 0 & 0 & \alpha_{66} & \beta_{66} \\ 0 & 0 & \beta_{66} & \delta_{66} \end{bmatrix} \begin{Bmatrix} N_z^i \\ M_z^i \\ N_{zs}^i \\ M_{zs}^i \end{Bmatrix} \tag{5}$$

Inverting Equation (5) we obtain a reduced constitutive equation for the i-th segment

$$\begin{Bmatrix} N_z^i \\ M_z^i \\ N_{zs}^i \\ M_{zs}^i \end{Bmatrix} = \begin{bmatrix} A_i & B_i & 0 & 0 \\ B_i & D_i & 0 & 0 \\ 0 & 0 & F_i & C_i \\ 0 & 0 & C_i & H_i \end{bmatrix} \begin{Bmatrix} \varepsilon_z^i \\ \kappa_z^i \\ \gamma_{zs}^i \\ \kappa_{zs}^i \end{Bmatrix} \tag{6}$$

The reduced constitutive equation [Equation (6)] is very important in this work. The segment stiffnesses A_i, B_i, D_i, F_i, C_i, and H_i allow for the determination of all the section properties needed to solve the general problem of bending and torsion. Note that the beam theory assumptions $N_s^i = M_s^i = 0$ do not preclude the deformations ε_s^i and κ_s^i which can be computed from the second and fifth equations in Equation (2).

A convenient numerical procedure to obtain directly the coefficients in Equation (6) is to statically condensate the second and fifth columns of Equation (1) (see Reference [32] pp. 450). A simple and efficient way is to reorder the rows and columns in Equation (1) so that the second and fifth rows and columns occupy the first two rows and columns. Then, interrupt the Gauss elimination process after the first two elements of the diagonal are equal to one.

A simple physical interpretation for the coefficients in Equation (6) can be obtained by using the expression for the stress resultants. For example, consider the inplane force per unit length

$$N_z^i = \int_{-t/2}^{t/2} \sigma_z dr \tag{7}$$

Taking into account that the behavior of each layer (denoted by the superscript k) in the laminate is elastic, we can write

$$\sigma_z = E_z^k(\varepsilon_z^i - r\kappa_z^i) \tag{8}$$

where E_z^k is the equivalent elastic modulus of layer k along the z-direction. Although the equivalent modulus E_z^k can be computed [24], it is not necessary to compute this value in order to perform the analysis described here because it is simpler to use Equation (1) through (6) or the static condensation procedure described previously. Performing the integration we obtain

$$N_z^i = A_i\varepsilon_z^i + B_i\kappa_z^i \tag{9}$$

with

$$\begin{aligned} A_i &= \int_{-t/2}^{t/2} E_z^k dr = \sum_{k=1}^{N} E_z^k t^k \\ B_i &= \int_{-t/2}^{t/2} r E_z^k dr = \sum_{k=1}^{N} E_z^k t^k \bar{r}^k \end{aligned} \tag{10}$$

where N is the number of layers in segment i, t^k is the thickness of layer k, r is the thickness coordinate, and $\bar{r}^k$ is the distance from the middle surface of the segment to the middle surface of layer k (see Reference [24] exercise 4.2.3). Clearly, A_i is the axial stiffness per unit length of the segment. The term B_i represents the coupling between bending curvature κ_z^i and extensional force per unit length N_z^i that appears when the laminate is not symmetric with respect to the midsurface of the segment. Using the expressions for the remaining stress resultants, it can be shown that

$$\begin{aligned} D_i &= \int_{-t/2}^{t/2} r^2 E_z^k dr = \sum_{k=1}^{N} E_z^k \left[\frac{(t^k)^3}{12} + t^k (\bar{r}^k)^2 \right] \\ F_i &= \int_{-t/2}^{t/2} G_{zs}^k dr = \sum_{k=1}^{N} G_{zs}^k t^k \\ H_i &= \int_{-t/2}^{t/2} r^2 G_{zs}^k dr = \sum_{k=1}^{N} G_{zs}^k \left[\frac{(t^k)^3}{12} + t^k (\bar{r}^k)^2 \right] \\ C_i &= \int_{-t/2}^{t/2} r G_{zs}^k dr = \sum_{k=1}^{N} G_{zs}^k t^k \bar{r}^k \end{aligned} \tag{11}$$

Here, D_i is the bending stiffness of the segment under bending M_z^i, F_i is the inplane shear stiffness under shear N_{zs}^i, H_i is the twisting stiffness under twisting moment M_{zs}^i, and C_i is the coupling between the twisting curvature κ_{zs}^i and the shear force per unit length N_{zs}^i [see Equation (6)] also called shear flow q. A simple

analogy with isotropic materials indicates that

$$\begin{aligned} A_i &= Et = EA/b \\ D_i &= Et^3/12 = EI/b \\ F_i &= Gt = GA/b \\ H_i &= Gt^3/12 = \frac{1}{4} GJ_R/b \end{aligned} \tag{12}$$

where E, G, t, b, and I are the elastic modulus, shear modulus, thickness, width, moment of inertia, and $J_R = bt^3/3$ for the isotropic material.

3.1 Principal Axis of Bending of the Segment

To investigate the physical significance of the term B_i, we propose a state of deformation $\varepsilon_z \neq 0$ with all the other strains and curvatures equal to zero. Then, the first two of Equation (6) become

$$\begin{aligned} N_z^i &= A_i \varepsilon_z^i \\ M_z^i &= B_i \varepsilon_z^i \end{aligned} \tag{13}$$

that can be solved to give

$$M_z^i = \frac{B_i}{A_i} N_z^i = e_b N_z^i \tag{14}$$

where

$$e_b = \frac{B_i}{A_i} \tag{15}$$

gives the location of the neutral surface of bending for the segment i. A force N_z^i acting with eccentricity $r = e_b$ (axis s') respect to the midsurface (contour s) in Figures 5 and 6, produces no bending curvature κ_z^i.

Once the location of the neutral axis of bending is known, the bending stiffness of the segment is computed with respect to the principal axis s' of the segment (Figure 5 and 6). Assuming that $N_z^i = 0$ and replacing the first equation in Equation (6) into the second equation, we obtain

$$M_z^i = \left(D_i - \frac{(B_i)^2}{A_i} \right) \kappa_z^i \tag{16}$$

and using Equation (15), we can write the bending stiffness per unit length of the segment as

$$\overline{D_i} = D_i - e_b^2 A_i \tag{17}$$

and the bending stiffness of the segment as

$$(EI_{s'}^i) = \overline{D_i} b_i \tag{18}$$

Note that we have multiplied by the segment width b_i so that the units of (EI) are $[Nm^2]$. Also note that (EI) cannot be separated into E and I as it is done for homogeneous isotropic materials.

The symbol (EI) indicates a single value (the bending stiffness), not a product of E times I. Two letters in parenthesis have been chosen instead of defining a new symbol so that the analogy between the present formulation and the case of isotropic materials discussed in classical textbooks [33,34] is apparent.

Therefore, the first two constitutive equations in Equation (6) become uncoupled

$$\begin{Bmatrix} N_z^i \\ M_z^i \end{Bmatrix} = \begin{bmatrix} A_i & 0 \\ 0 & \overline{D_i} \end{bmatrix} \begin{Bmatrix} \varepsilon_z^i \\ \kappa_z^i \end{Bmatrix} \tag{19}$$

when N_z^i, M_z^i, ε_z^i and κ_z^i are defined with respect to s'-axis (neutral surface of bending in Figure 6), with $\overline{D_i}$ given by Equation (17).

The resultant force corresponding to a strain ε_z constant through the thickness of the segment acts along the axis s' (which is on neutral surface of bending) on a point with coordinates (see Figure 6)

$$\begin{aligned} x(s') &= x(s) - e_b \sin \alpha_x^i \\ y(s') &= y(s) + e_b \cos \alpha_x^i \end{aligned} \tag{20}$$

where α_x^i is the angle of the segment with respect to axis x.

3.2 Principal Axis of Torsion of the Segment

To investigate the physical significance of the terms C_i we propose a state of deformation $\gamma_{zs}^i \neq 0$ and all other strain and curvatures equal to zero, the last two equations in Equation (6) also become uncoupled

$$\begin{aligned} N_{zs}^i &= F_i \gamma_{zs}^i \\ M_{zs}^i &= C_i \gamma_{zs}^i \end{aligned} \tag{21}$$

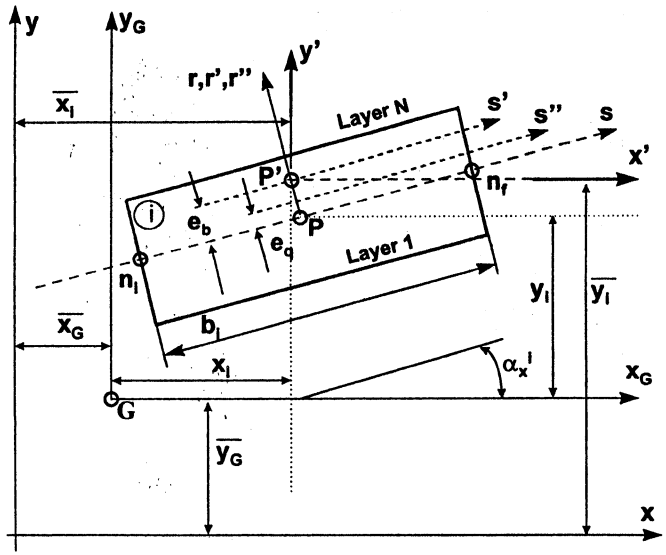

Figure 5. *Cross section of segment* i *showing the definition of the various variables.*

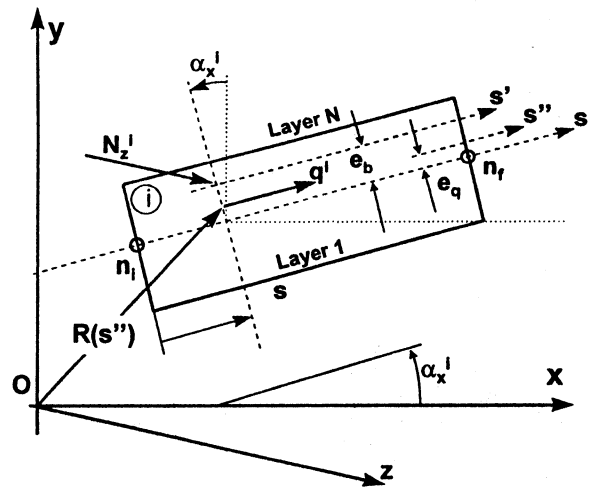

Figure 6. *Cross section of segment* i *showing the definition of the radius R.*

that can be solved to give

$$M_{zs}^i = e_q N_{zs}^i \tag{22}$$

with

$$e_q = \frac{C_i}{F_i} \tag{23}$$

that gives the location of the neutral axis of torsion for the segment i. A shear force N_{zs}^i acting with eccentricity $r = e_q$ (axis s'') respect to the midsurface (contour s) in Figure 6, produces only shear strain which is constant through the thickness. No twisting curvature κ_{zs}^i is induced by the lack of symmetry of the laminate in that segment.

Once the location of the neutral axis of torsion is known, the torsional stiffness of the segment is computed with respect to the principal axis of the segment s'' (Figure 5). Assuming that $N_{zs}^i = 0$ and replacing the third equation in Equation (6) into the fourth equation, we obtain the torsional stiffness per unit length of the segment as

$$\overline{H_i} = H_i - e_q^2 F_i \tag{24}$$

and the torsional stiffness of the segment as

$$(GJ_R^i) = 4\overline{H_i} b_i \tag{25}$$

where the factor 4 is explained in Section 4.4.1 [see Equation (46)].

Therefore, the last two equations of Equation (6) reduce to

$$\begin{Bmatrix} N_{zs}^i \\ M_{zs}^i \end{Bmatrix} = \begin{bmatrix} F_i & 0 \\ 0 & \overline{H_i} \end{bmatrix} \begin{Bmatrix} \gamma_{zs}^i \\ \kappa_{zs}^i \end{Bmatrix} \tag{26}$$

when N_{zs}^i, M_{zs}^i, γ_{zs}^i, and κ_{zs}^i are defined with respect to s''-axis (the neutral surface of torsion in Figures 5 and 6), with $\overline{H_i}$ given by Equation (24).

The shear flow corresponding to a shear strain γ_{zs}^i constant through the thickness acts on the neutral surface of torsion (axis s'') on a point with coordinates [see Figure (6)]

$$\begin{aligned} x(s'') &= x(s) - e_q \sin \alpha_x^i \\ y(s'') &= y(s) + e_q \cos \alpha_x^i \end{aligned} \tag{27}$$

4. SECTION PROPERTIES

The section properties are found integrating the stress components over the area of the cross section. The area integral is divided into an integral over the contour $\int_s(\,)ds$ and an integral over the thickness of the segment $\int_t(\,)dr$.

The material properties may vary from layer to layer and from segment to segment. Therefore, it is not possible to separate the elastic properties (E and G) from the geometric properties (area, moment of inertia, etc.). For this reason, in the following sections we define mechanical properties that contain the information of the geometry and the material combined. To illustrate this concept, consider a two-layer rectangular beam of width b and total thickness $2t$. The bottom layer has thickness t, density ρ_1, and modulus E_1. The top layer has $\rho_2 = 2\rho_1$ and $E_2 = 31E_1$. The geometric center of gravity of the cross section is found as $\bar{y}_G = \int_A y dA/\int_A dA$. It can be shown that $\bar{y}_G$ lays in the interface between the two layers regardless of the coordinate system used. Let's use a coordinate system with origin at the geometric center of gravity just found. The mass center of gravity is located at $\bar{y}_\rho = \int_A \rho y dA/\int_A \rho dA = t/6$. That is, the mass center of gravity is located at $t/6$ into the top layer, which is twice as dense as the bottom layer. The mechanical center of gravity is located at $\bar{y}_M = \int_A E y dA/\int_A E dA = 15/32t$. That is, the mechanical center of gravity almost coincides with the geometric and mass center of gravity of the top layer, which is 31 times stiffer than the bottom layer.

All mechanical properties are defined by integrals over the area of the cross-section. To define each one of the mechanical properties we solve first the integral over the thickness of the segment $\int_t(\,)dr$. The following comments can be made regarding the types of equilibrium integrals used in the rest of this section to obtain the mechanical section properties:

1. When computing bending moments produced by axial stresses, coordinates $x(s')$ and $y(s')$ [Equation (20)] will be used, meaning that the positions x and y on the neutral axis of bending are used.
2. When computing torque produced by shear stresses respect to a point O (Figure 6), coordinates $x(s'')$ and $y(s'')$ [Equation (27)] will be used to define the extreme of the radius $R(s'')$ in Figure 6.
3. Integrals used to compute equilibrium of forces do not contain the coordinates x and y. In those cases, neither Equation (20) nor Equation (27) will be needed.

While stiffeners can be modeled explicitly by adding them to the contour, it is sometimes convenient to use concentrated areas to represent them; thus reducing the complexity of the analysis. The contribution of concentrated areas is given by the axial stiffness (EA) and torsional stiffness (GJ_R) of the stiffener. These mechanical properties of the stiffener can be computed separately by modeling the stiffner with the present formulation [see Equation (30)]. In the computer implementation, a concentrated

area is entered as a segment with coinciding initial and final nodes. In this way, the contribution of the concentrated area is added to various integrals at the appropriate point (e.g., during the integration of mechanical static moment). Therefore, concentrated areas need not appear explicitly in the rest of the formulation. However, concentrated areas are accounted for when computing axial forces, bending moments, static moment, shear flow, twisting moments, etc.

4.1 Axial Stiffness

For simplicity, assume that a constant state of strain $\varepsilon_z^i = \varepsilon_z$ is applied and all other strains and curvatures are zero. Integrating the axial stress over the area of the cross section we get

$$N_z = \int_s \int_t \sigma_z dr ds = \int_s N_z^i(s')ds \tag{28}$$

and using Equation (19)

$$N_z = \int_s A_i \varepsilon_z^i ds = \varepsilon_z \int_s A_i ds = \varepsilon_z (EA) \tag{29}$$

where (EA) represents the axial stiffness of the section, ε_z the axial uniform strain of the beam, $\int_s$ indicates an integration over the contour describing the cross section. The contour integral reduces to adding the contribution of all the segments (Figure 1 through 3)

$$(EA) = \sum_{i=1}^{n} A_i b_i \tag{30}$$

where n is the number of segments describing the cross section. Note that (EA) cannot be separated into E and A as it is done for beams made of a single isotropic material. Note that the length of a segment is the same regardless of the contour used (s, s', or s'').

4.2 Mechanical Center of Gravity

The mechanical center of gravity of the cross section is the point of application of the axial force N_z, which is the resultant of the axial stresses caused by a constant state of strains ε_z. Equating moments respect to the x-axis

$$N_z \bar{y}_G = \int_s \int_t y(s')(\sigma_z dr ds) \tag{31}$$

and using Equation (19), (20) and (29) we have

$$\varepsilon_z(EA)\bar{y}_G = \varepsilon_z \int_s (y(s) + e_b \cos\alpha_x^i) A_i ds \tag{32}$$

Solving for $\bar{y}_G$ and repeating the same procedure for $\bar{x}_G$ we obtain

$$\begin{aligned} \bar{y}_G &= \frac{(ES_x)}{(EA)} \\ \bar{x}_G &= \frac{(ES_y)}{(EA)} \end{aligned} \tag{33}$$

where (ES_x) and (ES_y) are the mechanical static moments defined as

$$\begin{aligned} (ES_x) &= \int_s y(s') A_i ds = \sum_{i=1}^{n} \bar{y}_i A_i b_i \\ (ES_y) &= \int_s x(s') A_i ds = \sum_{i=1}^{n} \bar{x}_i A_i b_i \end{aligned} \tag{34}$$

and $\bar{x}_i$, $\bar{y}_i$, are the coordinates of the point P' (Figure 5) where $s = b_i/2$.

4.3 Principal Axes of Bending of the Beam

The product of the modulus of elasticity E times the moments of inertia I_x, I_y, and the product of inertia I_{xy} of classical beam theory are replaced by the mechanical properties of each segment defined as

$$\begin{aligned} (EI_{s'}^i) &= \overline{D_i} b_i \\ (EI_{r'}^i) &= A_i \frac{b_i^3}{12} \\ (EI_{r's'}^i) &= 0 \end{aligned} \tag{35}$$

Note that the bending stiffness $(EI_{s'}^i)$ was derived before [Equation (18)] and that the mechanical product of inertia $(EI_{r's'}^i)$ vanishes because the $s'r'$ are the principal axes of bending of the segment (Figure 5). The mechanical moments of inertia and the mechanical product of inertia of a segment with respect to axes $x'y'$ (Figure 5) are obtained by a rotation $-\alpha_x^i$ around z, as

$$\begin{aligned} (EI_{x'}^i) &= (EI_{s'}^i)\cos^2\alpha_x^i + (EI_{r'}^i)\sin^2\alpha_x^i \\ (EI_{y'}^i) &= (EI_{s'}^i)\sin^2\alpha_x^i + (EI_{r'}^i)\cos^2\alpha_x^i \\ (EI_{x'y'}^i) &= [(EI_{r'}^i) - (EI_{s'}^i)]\sin\alpha_x^i \cos\alpha_x^i \end{aligned} \tag{36}$$

Finally, using the parallel axis theorem and adding the contributions of all the segments, we obtain the mechanical moments of inertia and the mechanical product of inertia with respect to axes x_G, y_G,

$$\begin{aligned} (EI_{x_G}) &= \sum_{i=1}^{n} [(EI_{x'}^i) + A_i b_i (y_i + e_b \cos\alpha_x^i)^2] \\ (EI_{y_G}) &= \sum_{i=1}^{n} [(EI_{y'}^i) + A_i b_i (x_i - e_b \sin\alpha_x^i)^2] \\ (EI_{x_G y_G}) &= \sum_{i=1}^{n} [(EI_{x'y'}^i) + A_i b_i (y_i + e_b \cos\alpha_x^i)(x_i - e_b \sin\alpha_x^i)] \end{aligned} \tag{37}$$

where x_i, y_i are the coordinates of the center of segment i (point P in Figure 5) over the contour s ($r = 0$) with respect to the global system x_G, y_G. The system x_G, y_G has its origin at the mechanical center of gravity of the section and it is parallel to the global system x, y. In Equation (37), $(x_i - e_b \sin\alpha_x^i)$ and $(y_i + e_b \cos\alpha_x^i)$ are the coordinates of the center of the segment (point P' in Figure 5) over the axis s' ($r = e_b$).

The rotation ϑ locating the principal axes of bending η, ξ, with respect to the axes x_G, y_G, is found as usual by imposing the condition $(EI_{\eta\xi}) = 0$

$$\tan 2\vartheta = \frac{2(EI_{x_G y_G})}{(EI_{y_G}) - (EI_{x_G})} \tag{38}$$

and the maximum and minimum bending stiffness with respect to the principal axes of bending are

$$(EI_\eta);(EI_\xi) = \frac{(EI_{x_G}) + (EI_{y_G})}{2} \pm \sqrt{\left(\frac{(EI_{x_G}) + (EI_{y_G})}{2}\right)^2 + ((EI_{x_G y_G}))^2} \tag{39}$$

4.4 Torsional Stiffness

Taking into account the uncoupling between shearing and torsional effects in

Equation (26) when using principal axis of torsion s'', and noting that N^i_{zs} is the shear flow q^i we have

$$\begin{aligned} q^i &= F_i\gamma^i_{zs} \\ M^i_{zs} &= \overline{H}_i\kappa^i_{zs} \end{aligned} \tag{40}$$

Energy balance implies that the work done by external torque equals the strain energy due to shear

$$\frac{1}{2}T\beta L = \frac{L}{2}\int_s(\gamma^i_{zs}q^i + M^i_{zs}\kappa^i_{zs})ds \tag{41}$$

where β is the rate of twist. From Equation (40) and (41), it is possible to derive the torsional stiffness for both the open and closed section using the kinematic assumptions of the classical theory.

4.4.1 OPEN SECTION

For the open section, the shear flow vanishes ($q = 0$), so Equations (40) reduce to

$$\begin{aligned} q^i &= 0 \\ M^i_{zs} &= \overline{H}_i\kappa_{zs} \end{aligned} \tag{42}$$

Note that the superscript i has been dropped from κ_{zs} because the twisting curvature is unique for the section while the twisting moment varies from segment to segment. For the open section, the twisting curvature of classical plate theory is twice the twist rate β

$$\kappa_{zs} = 2\frac{\partial^2 w}{\partial z\partial s} = 2\beta \tag{43}$$

where w is the transverse deflection of the laminate. The energy balance [Equation (41)] can be written

$$T\beta = \int_s \overline{H}_i\kappa^2_{zs}ds = \kappa^2_{zs}\int_s \overline{H}_i ds \tag{44}$$

and using Equation (43) we have

$$\frac{T}{\beta} = 4\int_s \overline{H}_i ds \tag{45}$$

Since T/β is the torsional stiffness (GJ_R), we have

$$(GJ_R) = 4\sum_{i=1}^{n}\overline{H}_i b_i \tag{46}$$

For the isotropic case, Equation (46) leads to $J_R = 1/3\sum b_i t_i^3$.

4.4.2 SINGLE-CELL CLOSED SECTION

In this case $\kappa_{zs} = 0$ and Equations (40) reduce to

$$q^i = F_i\gamma^i_{zs} \tag{47}$$

$$M^i_{zs} = 0 \tag{48}$$

The energy balance [Equation (41)] reduces to

$$T\beta = \oint_s \gamma^i_{zs}q^i ds \tag{49}$$

Replacing Equation (47) in Equation (49) and taking into account that for a closed cell q is constant along the contour, we have

$$T\beta = q^2\oint_s \frac{ds}{F_i} \tag{50}$$

Equilibrium of moments can be used to obtain an expression for the torque T by integrating the shear flow over the contour s''

$$T = \oint_s (qR(s''))ds = q[2\Gamma_{s''}] \tag{51}$$

where $\Gamma_{s''}$ is the area enclosed by the contour s''.

The rate of twist β is determined dividing Equation (50) by Equation (51)

$$\beta = \frac{q}{2\Gamma_{s''}}\oint_s \frac{ds}{F_i} \tag{52}$$

The torsional stiffness is obtained dividing Equation (51) by Equation (52)

$$(GJ_R)_q = \frac{T}{\beta} = \frac{[2\Gamma_{s''}]^2}{\sum_{i=1}^{n}\frac{b_i}{F_i}} \tag{53}$$

The expression above can be improved to account for the nonuniform distribution of shear through the thickness of the laminate. This is done by adding the torsional stiffness of the open cell affected by a correction factor equal to 3/4 (see Appendix)

$$(GJ_R) = \frac{[2\Gamma_{s'}]^2}{\sum_{i=1}^{n} \frac{b_i}{F_i}} + \frac{3}{4}\left[4\sum_{i=1}^{n} \overline{H_i} b_i\right] \tag{54}$$

4.5 Shear of Open Sections

The analysis of shear stiffness, sectorial properties, shear center and restrained warping, must be considered separately for open and closed sections. To obtain these expressions, we must consider the shear flow caused by shear forces. As in the case of homogeneous materials, the shear flow caused by shear forces is obtained as an equilibrium condition using Jourawski's formula. But in the case of inhomogeneous materials, according to Equation (15) and (23), the resultant of axial forces that causes no bending curvature, and the resultant of shear flow that causes no twisting curvature act on different local axis. The same situation occurs in the case of restrained warping.

Note that consistently with classical thin wall beam theory, eccentricity effects e_b and e_q could be ignored, assuming the wall to be very thin. However, using e_b and e_q along with a linear variation of all the strains through the thickness, as provided by classical lamination theory [Equation (1)], it is possible to improve upon classical thin walled theory, modeling the thickness effects for moderately thick walls. Therefore, we will use the notation $\eta(s')$, $\xi(s')$, $r(s'')$, etc., [Equation (20) and Equation (27)] to indicate on what local axis the global coordinate is measured.

4.5.1 SHEAR FLOW CAUSED BY SHEAR FORCES

Using principal axes ξ, η (Figure 3), the shear flow caused by a shear force Q_η is given by Jourawski's formula (Reference [33] pp. 361) adapted for non homogeneous sections by replacing geometric properties by the mechanical properties used in this work. The first moment of the area at one side of the point where shear is evaluated is replaced by the mechanical static moment $(ES_\xi(s))$. The moment of inertia is replaced by the bending stiffness (EI_ξ), defined in Equation (39). Then, the shear flow is

$$q_\eta(s) = \frac{-Q_\eta (ES_\xi(s))}{(EI_\xi)} \tag{55}$$

where Q_η is the shear force applied in the direction η (Figure 3) and $(ES_\xi(s))$ is the mechanical static moment which is variable along the contour

$$(ES_\xi(s)) = \int_0^s \eta(s') A_i ds = \int_0^s (\eta(s) - e_b \sin\alpha_\eta^i) A_i ds \tag{56}$$

where α_η^i is the angle of the segment with respect to the principal axis η. This integral must start at the free end where $s = 0$. Note that the mechanical static moment $(ES_\xi(s))$ defined in Equation (56) is variable along the contour, while the values defined in Equation (34) are the total values for the beam cross section.

Integrating the shear flow caused by Q_η, and using Equation (55), we do not recover exactly Q_η. The difference grows with the thickness. A better approximation to $q_\eta(s)$ can be obtained by defining a consistent bending stiffness $(EI_\xi)^*$ to be used in Equation (55) so that equilibrium is satisfied

$$q_\eta(s) = \frac{-Q_\eta (ES_\xi(s))}{(EI_\xi)^*} \tag{57}$$

Integrating the forces originated by the shear flow we have

$$Q_\eta = \int_s (q_\eta(s)\, ds)\cos\alpha_\eta^i = \frac{-Q_\eta}{(EI_\xi)^*} \int_s (ES_\xi(s))\cos\alpha_\eta^i ds \tag{58}$$

Equation (58) is used to compute the consistent bending stiffness to be used in Jourawski's formula [Equation (57)]

$$(EI_\xi)^* = -\int_s (ES_\xi(s))\cos\alpha_\eta^i ds \tag{59}$$

Similarly

$$q_\xi(s) = \frac{-Q_\xi (ES_\eta(s))}{(EI_\eta)^*} \tag{60}$$

where

$$(ES_\eta(s)) = \int_0^s (\xi(s) + e_b \cos\alpha_\eta^i) A_i ds \tag{61}$$

$$(EI_\eta)^* = -\int_s (ES_\eta(s))\sin\alpha_\eta^i ds \tag{62}$$

Equations (59) and (62) are used to compute a consistent bending stiffness to improve Jourawski's formulas [Equation (57) and (60)]. This correction is gener-

ally overlooked in the literature for the isotropic case, but it is necessary for the case of beams with moderately thick walls.

4.5.2 SHEAR STIFFNESS OF THE SECTION

For an infinitesimal segment dz of the beam subject to shear Q_η, the balance between the external work and the strain energy is

$$\frac{1}{2}Q_\eta \gamma dz = \frac{1}{2}\frac{Q_\eta^2}{(GA_\xi)}dz = \frac{1}{2}\int_s (M_{zs}^I \kappa_{zs}^I + q^I \gamma_{zs}^I)\, ds dz \tag{63}$$

While the strain energy is computed as an integral over the volume, it must be noted that the integral over the thickness has already been computed in Equation (6). Taking into account only the shear deformations ($\kappa_{zs}^I = 0$), and using the third of Equation (6) and Equation (57) we have

$$\gamma_{zs}^i = \frac{q^i}{F_i} = \frac{-Q_\eta (ES_\xi(s))}{F_i (EI_\xi)^*} \tag{64}$$

Replacing into Equation (63) with $\kappa_{zs}^i = 0$, we obtain the shear stiffness of the section as

$$(GA_\xi) = \frac{[(EI_\xi)^*]^2}{\int_s [(ES_\xi(s))]^2 \frac{ds}{F_i}} \tag{65}$$

Similarly

$$(GA_\eta) = \frac{[(EI_\eta)^*]^2}{\int_s [(ES_\eta(s))]^2 \frac{ds}{F_i}} \tag{66}$$

4.5.3 SECTORIAL PROPERTIES

The sectorial area is defined in the usual form (Reference [33] pp. 307)

$$w(s) = \int_0^s R(s'')ds \tag{67}$$

using arbitrary points for the pole and for the initial point where $w(s) = 0$ (Figure 2). The radius R in Equation (67) (see Figure 6) must be evaluated on the local axis

s'' because $dw(s)$ will be used to define twisting moment caused by shear flow (acting on s'') in Equation (72) through Equation (76).

In the case of open sections, Equation (67) may require to treat the segments in a different order of that used initially to define the contour (Table 2), because we can start to compute a segment only if the value of $\omega(s)$ in either extreme is already known. In Figure 2(b), we add sequentially the static moment of segments 1, 2,. . .,6. To compute sectorial area the order is 1, 3, 2, 4 . . .6.†

The sectorial area $w(s)$ is used in the definition of the mechanical sectorial properties, which are defined as follows:

The mechanical sectorial static moment

$$(Ew) = \int_s w(s) A_i ds \tag{68}$$

The mechanical sectorial linear moments

$$(ESw_\xi) = \int_s (\eta(s) - e_b \sin \alpha_\eta^i) w(s) A_i ds \tag{69}$$

and

$$(ESw_\eta) = \int_s (\xi(s) + e_b \cos \alpha_\eta^i) w(s) A_i ds \tag{70}$$

The mechanical sectorial moment of inertia

$$(EIw) = \int_s [w(s)]^2 A_i ds \tag{71}$$

4.5.4 MECHANICAL SHEAR CENTER

The coordinate ξ_c of the mechanical shear center is calculated by equilibrium of moments (with respect to the mechanical center of gravity), caused by the shear force Q_η and its associated shear flow $q_\eta(s)$ [defined in Equation (57)]

$$Q_\eta \xi_c = \int_I^F R(s'') q_\eta(s) ds \tag{72}$$

where the initial point I is at the free end and F is the final point (Figure 2). Using Equation (57) and (56) into (72) we have

†The current computer implementation reorders segments automatically.

$$\xi_c = \frac{-1}{(EI_\xi)^*} \int_I^F R(s'')\left[\int_I^s \eta(s')A_i ds\right] ds \tag{73}$$

Recognizing that $[R(s'')ds]$ is the differential of sectorial area $dw(s)$ and that $[\eta(s')A_i ds]$ is the differential of mechanical static moment $d(ES_\xi(s))$, the order of integration can be changed (integration by parts). Since the mechanical static moment is zero at the end points we have

$$\xi_c = \frac{-1}{(EI_\xi)^*} \int_I^F \eta(s')A_i\left[\int_I^s dw\right] ds = \frac{-1}{(EI_\xi)^*} \int_I^F \eta(s')A_i w(s) ds \tag{74}$$

and using Equation (69)

$$\xi_c = -\frac{(ESw_\xi)}{(EI_\xi)^*} \tag{75}$$

The pole of the sectorial area $w(s)$ is the mechanical center of gravity because in Equation (72) the moments are taken respect to the point (x_G, y_G). Similarly

$$\eta_c = -\frac{(ESw_\eta)}{(EI_\eta)^*} \tag{76}$$

It is important to note that if we use the mechanical shear center as pole, then $\xi_c = 0$ and $\eta_c = 0$. Therefore, by Equation (75) and (76), the mechanical sectorial linear moments are zero.

4.5.5 RESTRAINED WARPING

Secondary Forces. When free warping due to torsion is restrained, axial secondary forces appear. They can be computed (Reference [33] Section 8.11) as

$$N_z(s) = -\frac{d^2\theta}{dz^2} \overline{w}(s)A_i \tag{77}$$

where $\overline{w}(s)$ is the principal sectorial area as will be shown in the next section. Equilibrium of forces requires a secondary shear flow

$$q_w(s) = \frac{d^3\theta}{dz^3} \int_0^s \overline{w}(s)A_i ds \tag{78}$$

The angle of twist θ is computed solving the general equation for torsion

$$\frac{d^4\theta}{dz^4} - k^2 \frac{d^2\theta}{dz^2} = -k^2 \frac{T'}{(GJ_R)} \tag{79}$$

where $T' = dT/dz$, and $k^2 = (GJ_R)/(EI\,\overline{w})$, and $(EI\,\overline{w})$ is the mechanical warping stiffness defined as in (Reference [33] pp. 320) which is computed as in Equation (71) but using principal sectorial area

$$(EI\,\overline{w}) = \int_s [\overline{w}(s)]^2 A_i ds \tag{80}$$

Principal Sectorial Area Diagram. In the case of torsion T acting alone, the secondary axial forces integrated in the contour s' must vanish because no axial force N_z is applied

$$N_z = \int_s N_z(s) ds = 0 \tag{81}$$

and using Equation (77) leads to

$$\int_s \overline{w}(s)A_i ds = 0 \tag{82}$$

The bending moments M_ξ and M_η caused by the secondary axial forces must also vanish. Using Equation (77), the conditions $M_\xi = 0$ and $M_\eta = 0$ lead to

$$\int_s (\eta(s) - e_b \sin\alpha_\eta^i)\overline{w}(s)A_i ds = 0 \tag{83}$$

$$\int_s (\xi(s) + e_b \cos\alpha_\eta^i)\overline{w}(s)A_i ds = 0 \tag{84}$$

These equations can be satisfied, using an arbitrary initial point, if the mechanical shear center is used as a pole. As it was seen at the end of Section 4.5.4, the left hand side of Equation (83) and (84), which are mechanical sectorial linear moments [Equation (69) and (70)] will vanish. To satisfy Equation (82) the initial point is changed, which is equivalent to subtracting a constant. To obtain the principal sectorial area $\overline{w}(s)$, a sectorial area $w_1(s)$ with an arbitrary initial point is calculated first. The mechanical shear center is used as the pole to also satisfy Equation (83) and (84)

$$w_1(s) = \int_I^s R(s'') ds \tag{85}$$

where, as in Equation (67) the end of the radius R is located on the axis s'' (Figure 6). Then, the principal sectorial area $\overline{w}(s)$ is defined as

$$\overline{w}(s) = w_1(s) - w_0 \tag{86}$$

where the constant w_0 is obtained after introducing Equation (86) into Equation (82), or

$$w_0 = \frac{1}{(EA)} \int_s w_1(s) A_i ds \tag{87}$$

4.6 Shear of Single Cell Closed Section

4.6.1 SHEAR FLOW CAUSED BY SHEAR FORCES

For closed sections, the point at which $q(s) = 0$ is not known a priori. Therefore, to use Jourawski's formula [Equation (57)], it is necessary to proceed in two steps. First, consider the shear force Q_η acting on the mechanical shear center which does not produce shear flow by torsion, and apply Equation (57) using an arbitrary initial point.

$$q_{1\eta}(s) = -\frac{Q_\eta (ES_\xi(s))}{(EI_\xi)^*} \tag{88}$$

To change the initial point is equivalent to add a constant $q_{0\eta}$ such that

$$q_\eta(s) = q_{1\eta}(s) + q_{0\eta} \tag{89}$$

Since the shear load was applied at the mechanical shear center, the constant $q_{0\eta}$ must be such that the section does not rotate due to torsion. The rate of twist due to torsion is given by Equation (52). Since the shear flow due to shear [Equation (89)] is not constant, we have (see Reference [33] pp. 371)

$$\beta = \frac{1}{2\Gamma_{s'}} \oint_s (q_{1\eta}(s) + q_{0\eta}) \frac{ds}{F_i} \tag{90}$$

Setting $\beta = 0$ leads to

$$q_{0\eta} = -\oint_s q_{1\eta}(s) \frac{ds}{F_i} \Big/ \oint_s \frac{ds}{F_i} \tag{91}$$

Similarly, the shear flow caused by Q_ξ can be obtained as

$$q_\xi(s) = q_{1\xi}(s) + q_{0\xi} \tag{92}$$

where

$$q_{1\xi}(s) = -\frac{Q_\xi (ES_\eta(s))}{(EI_\eta)^*} \tag{93}$$

and

$$q_{0\xi} = -\oint_s q_{1\xi}(s) \frac{ds}{F_i} \Big/ \oint_s \frac{ds}{F_i} \tag{94}$$

4.6.2 MECHANICAL SHEAR CENTER

The coordinate ξ_c of the mechanical shear center is calculated by equilibrium of moments (with respect to the mechanical center of gravity), caused by the shear force Q_η and its associated shear flow $q_\eta(s)$ (Figure 6)

$$Q_\eta \xi_c = \oint_s q_\eta(s) R(s'') ds \tag{95}$$

or using Equation (89)

$$\xi_c = \frac{1}{Q_\eta} \oint_s (q_{1\eta}(s) + q_{0\eta}) R(s'') ds \tag{96}$$

where $q_{1\eta}(s)$ is given by Equation (88) and $q_{0\eta}$ is given by Equation (91). Similarly

$$\eta_c = \frac{1}{Q_\xi} \oint_s (q_{1\xi}(s) + q_{0\xi}) R(s'') ds \tag{97}$$

4.6.3 SHEAR STIFFNESS OF THE SECTION

The derivation is similar to that of Equation (63–66). However, for the closed section, the point where the mechanical static moment is zero is not known a priori. This problem is addressed similarly to Section 4.6.2. For the case of a unit applied shear load $Q_\eta = 1$, Equation (63) leads to

$$(GA_\xi) = 1 \Big/ \oint_s \frac{[q_\eta(s)]^2}{F_i}\, ds$$
$$(GA_\eta) = 1 \Big/ \oint_s \frac{[q_\xi(s)]^2}{F_i}\, ds \tag{98}$$

where it was assumed that $\kappa^i_{zs} = 0$ and $\gamma^i_{zs} = q/F_i$ as it was done in Equation (64), $q_\eta(s)$ is defined in Equation (89), and $q_\xi(s)$ is defined in Equation (92).

4.6.4 SHEAR FLOW CAUSED BY TORSION

The shear flow due to torsion is obtained from Equation (51)

$$q_T = \frac{T}{2\Gamma_{s'}} \tag{99}$$

Equation (99) applies for very small thickness. When the thickness is not that small, a better result can be obtained recognizing that part of the moment is in equilibrium because of the Saint Venant stresses, like in the open section. The total torsional moment (T) is distributed among shear flow (T_q) and the Saint Venant stresses (T_{SV})

$$T = T_q + T_{SV} \tag{100}$$

The distribution is proportional to the respective stiffness, according to

$$\frac{T}{(GJ_R)} = \frac{T_q}{(GJ_R)_q} = \frac{T_{SV}}{\frac{3}{4}(GJ_R)_{SV}} \tag{101}$$

where (GJ_R) is given by Equation (54), $(GJ_R)_q$ is given by Equation (53), $(GJ_R)_{SV}$ is given by Equation (46) and the correction factor 3/4 for a circular tube is used as in Equation (54). Introducing Equation (101) into Equation (100) yields

$$T_q = T - T_{SV} = T\left[1 - \frac{3}{4}\frac{(GJ_R)_{SV}}{(GJ_R)}\right] \tag{102}$$

Recognizing that T_q produces q_T in Equation (99), we have

$$q_T = \frac{T}{2\Gamma_{s'}}\left[1 - \frac{3}{4}\frac{(GJ_R)_{SV}}{(GJ_R)}\right] \tag{103}$$

It is important to note that in the case of an isotropic circular tube, the theory developed here [Equation (54), (103), (107), etc.) gives the exact result for stiffness and strength regardless of the thickness.

5. BEAM DEFORMATIONS

The deformations of the beam are now computed using the classical formulas referred to the principal axes. Therefore, the axial strain ε_z, the two curvatures κ_η, κ_ξ, and the twist ratio β are computed as follows

$$\varepsilon_z = \frac{N_z}{(EA)}$$
$$\kappa_\eta = \frac{M_\eta}{(EI_\eta)}$$
$$\kappa_\xi = \frac{M_\xi}{(EI_\xi)} \tag{104}$$
$$\beta = \frac{T}{(GJ_R)}$$

If the beam is a component of a structural system (indeterminate or not), the mechanical properties (EA), (EI_η), (EI_ξ), (GA_η), (GA_ξ), and (GJ_R), can be easily transformed into equivalent geometrical properties (dividing by arbitrary equivalent modulus E and G). The nodal displacements of the structure and stress resultants at any section can be obtained using the equivalent properties as input for any structural analysis program, either a beam finite element analysis or a matrix structural analysis program. Later on, these stress resultants can be used in Equation (104) to compute the beam deformations at any section of the structure. The proposed theory and its computer implementation can be used as a pre- and post-processor for any standard matrix structural analysis program.

6. SEGMENT DEFORMATIONS AND STRESSES

The axial strain in the midsurface at any point can be computed in terms of the beam deformations [Equation (104)]

$$\varepsilon^i_z(s) = \frac{N_z}{(EA)} + \xi(s)\frac{M_\eta}{(EI_\eta)} - \eta(s)\frac{M_\xi}{(EI_\xi)} - \frac{d^2\theta}{dz^2}\bar{w}(s) \tag{105}$$

where the last term correspond to restrained warping [Equation (77)] for an open

section. Note that $\varepsilon_z^i(s)$ changes point to point because $\xi(s)$ and $\eta(s)$ are the coordinates in principal axis of a point in the contour s, and $\overline{w}(s)$ also changes with s.

The bending curvature, which is unique for each segment, can also be computed in terms of the beam deformations [Equation (104)]

$$\kappa_z^i = \kappa_\eta \cos\alpha_\eta^i + \kappa_\xi \sin\alpha_\eta^i \tag{106}$$

where α_η^i is the angle between the segment with i orientation and the principal axis η. The twisting curvature, constant for all segments, is calculated from the twist rate β

$$\kappa_{zs}^i = \begin{Bmatrix} -2T/(GJ_R) & \text{open section} \\ -T/(GJ_R) & \text{closed section} \end{Bmatrix} \tag{107}$$

where the minus sign is introduced to account for the definition of the positive torque T in Figure 1 and the positive twisting moment M_{zs}^i in Figure 4.

To determine the shear strain $\gamma_{zs}^i(s)$, we need first to obtain the total shear flow from shear, torsion, and restrained warping, acting in the local s'' axis

$$q(s) = q_\eta(s) + q_\xi(s) + q_T + q_W(s) \tag{108}$$

where the last term in Equation (108) correspond to a restrained warping [Equation (78)]. The shear flow $q_\eta(s)$ due to shear forces Q_η is given by Equation (57) and Equation (89) for open and closed sections respectively. The shear flow $q_\xi(s)$ due to shear force Q_ξ is given by Equation (60) for open sections and Equation (92) for closed sections. The constant flow due to torsion q_T is given by Equation (103) for closed sections and $q_T = 0$ for open sections.

The shear strain $\gamma_{zs}^i(s)$ in the midsurface can be calculated from the third equation in Equation (6)

$$\gamma_{zs}^i(s) = \frac{N_{zs}^i - C_i\kappa_{zs}^i}{F_i} = \frac{q(s)}{F_i} - e_q^i\kappa_{zs}^i \tag{109}$$

where $q(s)$ is given by Equation (108) and κ_{zs}^i is given by Equation (107). Note that the shear flow acting on s'' does not produce curvature; the curvature in Equation (109) is due to torsion only.

Finally, the stress resultants are computed at each point by Equation (6). The four stress resultants are complemented with $N_s^i = 0$ and $M_s^i = 0$, reordered, and introduced in a standard laminate analysis program [using Equation (1)] to evaluate

the failure criteria. Three failure criteria were implemented in this work: the maximum stress, maximum strain, and Tsai-Wu quadratic interaction criteria. These computations are repeated for as many points in each segment of the contour as necessary to verify that the stresses do not exceed the allowable values.

It is interesting to note that using Equation (107) and (109) in the third and fourth equation of Equation (6) we get as expected

$$\begin{aligned} N_{zs}^i &= q(s) \\ M_{zs}^i &= e_q q(s) + \overline{H}_i\kappa_{zs}^i \end{aligned} \tag{110}$$

Equation (1) is derived under the assumption of linear strain distribution through the thickness. While classical thin walled beam theory can account for bending effects, the shear strain caused by torsion in closed cells is constant through the thickness, which limits the formulation to thin walls. On the other hand, the present formulation provides a better approximation by using a linear distribution of shear through the thickness. Therefore, it is possible to analyze moderately thick walls, which are not so thick as to require the inclusion of transverse shear effects. However, the shear stress distribution in the walls due to shear forces [$q_\eta(s) + q_\xi(s)$ in Equation (108)] are still considered constant through the thickness.

7. NUMERICAL RESULTS

Numerical results obtained using the procedure developed in this paper are compared in this section to experimental results from the literature. Experimental results for rectangular tubes made of Graphite-Epoxy are reported in Reference [22] and analyzed in Reference [23]. They present results for a box beam of length $L = 76.2$ cm, clamped at one end and with a tip torque $T = 0.113$ Nm applied at the other end. The external dimensions of the cross section were: height $d = 26.035$ mm and width $c = 52.324$ mm. The laminate of all walls was a cross-ply with 6 layers, each 0.127 mm thick, in a $[0/90]_3$ configuration, with a total thickness of 0.762 mm. The elastic properties of each ply were $E_L = 141.865$ GPa, $E_T = 9.784$ GPa, $G_{LT} = 5.994$ GPa, and $\nu_{LT} = 0.42$. Note that the laminate is not symmetric but the cross section is symmetric since the interior layer has the same angle in all walls of the cross section. While, the reported experimental angle of twist at the tip was 0.420 10^{-3} rad., the model developed in this paper predicts 0.426 10^{-3} rad., with a 1.4% difference.

Experimental results for laminated circular pipe are presented in Reference [21] along with analytical and finite element analysis of the circular pipe. The pipe was constructed of 30 layers, each 0.254 mm thick, of hand lay-up fiberglass and arranged in a cross-ply unsymmetric configuration $[0/90]_{15}$. The material properties were reported as $E_L = 16.605$ GPa, $E_T = 7.028$ GPa, $G_{LT} = 2.315$ GPa, and $\nu_{LT} =$

0.2403. The mean radius of the pipe was $R = 5.334$ cm and the length $L = 1.219$ m. It should be noted that nonlinear behavior was observed for high values of torque. However, with an applied torque of 1356 Nm the material remained in the linear range. Under these conditions, a twist angle of 5.77 degrees was measured and 5.60 degrees was predicted using the theory in this paper, with a 3% difference. Also for 1356 Nm of applied torque, a shear strain of 3675 microstrain (microstrain = 10^{-6} mm/mm) was measured on the surface of the pipe. The analysis presented in Reference [21] predicted a shear strain of 4316 microstrain while 4278 microstrain was predicted at the mid-surface using the theory in this paper. The strain at the outer surface can be computed as $\gamma_{zs} + \kappa_{zs}\, t/2 = 4580$ microstrain. The discrepancy between experimental and theoretical strains may be caused by uncertainties in the material properties.

8. CONCLUSIONS

The concept of mechanical properties was introduced in this paper to substitute the product of the modulus of elasticity times the geometrical properties used in classical textbooks. With certain care to model the laminated structure of the material, it was shown that it is possible to follow closely the theory of beams presented in classical strength of materials textbooks. This has the advantage that thin-walled composite beam theory becomes accessible to a large number of engineers that are familiar with the subject. By transforming the mechanical properties into equivalent geometrical properties (dividing by arbitrary values of E and G), the present formulation can be used as a pre- and post-processor of any matrix structural analysis program. All the contour integrals are reduced to summations over the number of segments, allowing for a general solution for any geometry of the cross section, open or closed, without the need for specialized evaluation of contour integrals. Comparisons with experimental data show good correlation, consistent with the assumptions of the theory. The formulation presented in this paper can be easily extended to multicell sections and closed cells with fins. Finally, constrained warping of closed cells can be easily added, although it is usually negligible.

APPENDIX. CORRECTION TERM IN EQUATION (54)

In Equation (49), the shear strain γ_{zs} is constant through the thickness because of the assumptions of classical plate theory [24]. For an isotropic section, this translates into τ_{zs} = constant, which is commonly accepted in thin walled theory. For the particular case of a tubular section, the exact solution of torsion is available, and it reveals a linear variation of τ_{zs} through the thickness. Comparing the exact solution for the tubular section of mean diameter D and thickness t

$$(GJ_R)_{exact} = \frac{\pi}{4} Dt(D^2 + t^2)G$$

with the result for a thin walled tube obtained using Bredt formula [33,34]

$$(GJ_R)_{Bredt} = \frac{\pi}{4} Dt(D^2)G$$

and the formula for a tube with a longitudinal slit (open section)

$$(GJ_R)_{open} = \frac{4}{3}\left[\frac{\pi}{4} Dt(t^2)G\right]$$

it is clear that the thin walled solution for closed tube is missing 3/4 of the open section solution to reach the exact solution for the tube.

REFERENCES

1. Barbero, E. J., Applications: Construction, in Lubin's Handbook of Composites, 2nd. Ed., Stan Peters, Editor, Van Nostrand, Reinhold, N. Y., 1998.
2. Savoia, M. and Tullini, N., Torsional Response of Inhomogeneous and Multilayered Composite Beams, Composite Structures, 25(1993) 587–594.
3. Muskhelishvili, N. J., Some Basic Problems of the Theory of Elasticity, 4th Ed., Noordhoff, The Netherlands, 1963.
4. Cheng, S., Wei, X., and Jiang, T., Stress Distribution and Deformation of Adhesive-Bonded Laminated Composite Beams, J. Eng. Mech., ASCE, 115 (1989) 1150–1162.
5. Lekhnitskii, S. T., Theory of Elasticity of Anisotropic Elastic Body, Holden-Day, San Francisco, CA, 1963.
6. Whitney, J. M. and Kurtz, R. D., Analysis of Orthotropic Laminated Plates Subjected to Torsional Loading, Composites Engineering, Vol. 3, No 1, pp. 83–97, 1993.
7. Whitney, J. M., Analysis of Anisotropic Laminated Plates Subjected to Torsional Loading, Composites Engineering, Vol. 3, No 6, pp. 567–582, 1993.
8. Skudra, A. M., Bulavs, F., Ya., Gurvich, M. R. and Kruklinsh, A. A., Structural Analysis of Composite Beam Systems, Technomic, Lancaster, PA, 1991.
9. Sankar, B. V., Beam Theory for Laminated Composites and Application to Torsion Problems, J. Appl. Mech., ASME, 60 (1993) 246–249.
10. Tsai, C. L., Daniel, I. M., and Yaniv, G., Torsional Response of Rectangular Composite Laminates, J. Appl. Mech., ASME, 57 (1990) 383–387.
11. Vasiliev, V. V., 1993, Mechanics of Composite Structures, Taylor and Francis, Bristol, PA.
12. Hong, C-H. and Chopra, I., Aeroelastic Stability Analysis of a Composite Rotor Blade, J. Amer. Helicopter Soc. 30(2), 1985.
13. Librescu, L. and Kehdir, A. A., Aeroelastic Divergence of Swept-Forward Composite Wings Including Warping Restraint Effects, AIAA Journal, 26(11), 1988.
14. Reissner, E. and Tsai, W. T., Pure Bending, Stretching, and Twisting of Anisotropic Cylindrical Shells, J. Applied Mechanics, 1972.

15. Mansfield, E. H. and Sobey, A. J., The Fibre Composite Helicopter Blade; Part I: Stiffness Properties; Past II: Prospects for Aeroelastic Tailoring, Aeronautical Quarterly, 30(2), 1979.
16. Rehfield, L. W., Altigan, A. R., and Hodges, D. H., Non-Classical Behavior of Thin-Walled Composite Beams with Closed Cross Sections, J. Amer. Helicopter Society, 35(2), 1990.
17. Bachau, O. A., A Beam Theory for Anisotropic Materials, J. Appl. Mech., Vol. 52, 1985.
18. Libove, C., Stresses and Rate of Twist in Single-Cell Thin-Walled Beams with Anisotropic Walls, AIAA J., Vol. 26, 1988.
19. Bicos, A. S. and Springer, G. S., Design of a Composite Box Beam, J. Comp. Mater., Vol. 20, 1986.
20. Minguet, P. and Dugundji, J., Experiments and Analysis for Composite Blades Under Large Deflections; Part I: Statics; Part II: Dynamics, AIAA J., 28(9), 1990.
21. Zhao, Y. and Pang, S. S., 1995, Stress-Strain and Failure Analyses of Composite Pipe Under Torsion, J. Pressure Vessel Technology, 117 (August), 273–278.
22. Chandra, R., Stemple, A. D. and Chopra, I., 1990, Thin-Walled Composite Beams Under Bending, Torsional, and Extensional Loads, Journal of Aircraft, 27(7).
23. Smith, E. C. and Chopra, I., 1991, Formulation and Evaluation of an Analytical Models for Composite Box-Beams, J. of Amer. Helicopter Society, 23–35, (7).
24. Jones, R. M., 1975, Mechanics of Composite Materials, Taylor and Francis, Bristol, PA.
25. Barbero, E. J., 1999, Introduction to Composite Materials Design, Taylor and Francis, Bristol, PA.
26. Tsai, S. W., 1988, Composites Design, Think Composites, Dayton, OH.
27. Wu, X. X. and Sun, C. T., 1990, Vibration Analysis of Laminated Composite Thin Walled Beams Using Finite Elements, AIAA Journal, 29, 736–742.
28. Barbero, E. J., Lopez-Anido, R., and Davalos, J. F., Mechanics of Laminated Beams, J. Composite Materials, 28(8), 806–829, (1993).
29. Lopez-Anido, R., Davalos, J. F. and Barbero, E. J. "Experimental Evaluation of Stiffness of Laminated Composite Beam Elements under Flexure," J. Reinforced Plastics and Composites, 14(4), 349–361, (1995).
30. Davalos, J. F., Salim, H. A., Qiao, P., Lopez-Anido, R. and Barbero, E. J., "Analysis and Design of Pultruded FRP Shapes under Bending," Composites Part B, 27B, 295–305, 1996.
31. Davalos, J. F., Qiao, P., and Barbero, E. J., Multiobjective Materials Architecture Optimization of Pultruded FRP I-Beams, Composite Structures, 35(3), 271–281, 1996.
32. Bathe, K-J., 1982, Finite Element Procedures in Engineering Analysis, Prentice Hall, New Jersey.
33. Cook, R. D. and Young W. C., 1985, Advanced Mechanics of Materials, Macmillan, New York.
34. Boresi, A. P., R. J. Schmidt, and Sidebottom, O. M., 1993, Advanced Strength of Materials, 5th Ed., Wiley, New York.
35. Young, W. C., Roark's Formulas for Stress and Strain, McGraw Hill, N. Y., 1989.

Experimental Evaluation of Repair Efficiency of Composite Patching by ESPI

WEI-CHUNG WANG*
Department of Power Mechanical Engineering
National Tsing Hua University
Hsinchu, Taiwan 30043
Republic of China

TSANN-BIM CHIOU
National Nano Device Laboratories
National Science Council
Hsinchu, Taiwan 30043
Republic of China

(Recieved October 24, 1997)
(Revised March 28, 1998)

ABSTRACT: In this paper, the electronic speckle pattern interferometry (ESPI) technique was first used to investigate repair efficiency of patching by using composite materials on aluminum alloy plates containing a central crack. The effect of single-sided and double-sided patchings with same total thickness and four different fiber orientations of the patchings was discussed. A self-developed computer program for analyzing mode I stress intensity factor (SIF), K_I, was performed to evaluate the repair efficiency. To verify the correctness of the experimental results, recontruction technique was employed. Well-matched condition between the experimentally obtained and reconstructed fringes indicates the correctness of the experimental results.

KEY WORDS: electronic speckle pattern interferometry, stress intensity factor, composite patching.

1. INTRODUCTION

IN THE PROCESS of manufacturing or applications, damages are occasionally produced in structures or structural components. When the damages appear in a part of structure or an important component of a structure while the structure or the

*Author to whom correspondence should be addressed.

0021-9983/98/17 1595–22 $10.00/0